NANO LETTERS
Letter
Cite This: Nano Lett. 2020, 20, 953−962
pubs.acs.org/NanoLett

Few-Wall Carbon Nanotube Coils

Dekel Nakar,[†] Georgy Gordeev,[‡] Leonardo D. Machado,[§] Ronit Popovitz-Biro,[⊥] Katya Rechav,[⊥] Eliezer F. Oliveira,[∥,#] Patryk Kusch,[‡] Ado Jorio,[¶] Douglas S. Galvão,[∥,#] Stephanie Reich,[‡] and Ernesto Joselevich*[,†]

[†]Department of Materials and Interfaces, Weizmann Institute of Science, Rehovot 7610001, Israel
[‡]Department of Physics, Freie Universität Berlin, 14195 Berlin, Germany
[§]Department of Theoretical and Experimental Physics, Federal University of Rio Grande do Norte, Natal, Rio Grande do Norte 59078-970, Brazil
[⊥]Department of Chemical Research Support, Weizmann Institute of Science, Rehovot 7610001, Israel
[∥]Applied Physics Department, State University of Campinas − UNICAMP, Campinas, São Paulo 13083-859, Brazil
[#]Center for Computational Engineering and Sciences (CCES), State University of Campinas − UNICAMP, Campinas, São Paulo 13083-859, Brazil
[¶]Departamento de Física, Universidade Federal de Minas Gerais, Belo Horizonte, Minas Gerais 31270-901, Brazil

Supporting Information

ABSTRACT: While various electronic components based on carbon nanotubes (CNTs) have already been demonstrated, the realization of miniature electromagnetic coils based on CNTs remains a challenge. Coils made of single-wall CNTs with accessible ends for contacting have been recently demonstrated but were found unsuitable to act as electromagnetic coils because of electrical shorting between their turns. Coils made of a few-wall CNT could in principle allow an insulated flow of current and thus be potential candidates for realizing CNT-based electromagnetic coils. However, no such CNT structure has been produced so far. Here, we demonstrate the formation of few-wall CNT coils and characterize their structural, optical, vibrational, and electrical properties using experimental and computational tools. The coils are made of CNTs with 2, 3, or 4 walls. They have accessible ends for electrical contacts and low defect densities. The coil diameters are on the order of one micron, like those of single-wall CNT coils, despite the higher rigidity of few-wall CNTs. Coils with as many as 163 turns were found, with their turns organized in a rippled raft configuration. These coils are promising candidates for a variety of miniature devices based on electromagnetic coils, such as electromagnets, inductors, transformers, and motors. Being chirally and enantiomerically pure few-wall CNT bundles, they are also ideal for fundamental studies of interwall coupling and superconductivity in CNTs.

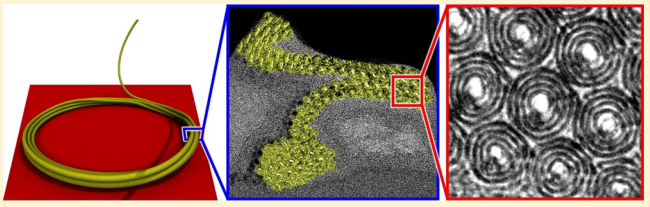

KEYWORDS: *carbon nanotubes, multiwall carbon nanotubes, coil, self-organization, transmission electron microscope, Raman, molecular dynamics*

Carbon nanotubes (CNTs) have attracted tremendous scientific and technological attention because of their extraordinary electrical, mechanical, and other properties, which make them attractive building blocks for nanotechnology.[1] Various nanoelectronic components made of CNTs have been proposed and demonstrated, including transistors,[2] diodes,[3] capacitors,[4] and entire nanocomputer prototypes.[5] Induction coils are basic components in electronic circuits, as well as in many macroscopic electrical and electromechanical devices. However, a micrometer-scale coiled CNT structure that can act as an inductive coil has yet to be produced. Such a structure could potentially be the basis for a series of miniature devices including electromagnets, inductors, dynamos, transformers, and motors.

The spontaneous coiling of flexible rods is a widespread phenomenon found in both macro and micro scales, such as cooked spaghetti,[6] viscous jets of honey or silicones,[7−9] supercoiled DNA,[10] and CNTs.[11−13] Various coiled CNT structures have been demonstrated, but a CNT coil suitable for the production of micrometer-scale electromagnetic coils has yet to be shown. For instance, previously reported helical CNTs were based on periodic pentagon-heptagon defects.[14] Such defects are known to scatter electrons and thus alter the electronic properties of the CNTs.[3,15] In addition, such coils are usually not compact but rather have a high ratio of interturn pitch to diameter, forming long and narrow solenoids. Other coiled CNTs "CNT rings" were formed by

Received: September 26, 2019
Revised: December 19, 2019
Published: December 23, 2019

DOI: 10.1021/acs.nanolett.9b03977
Nano Lett. 2020, 20, 953−962

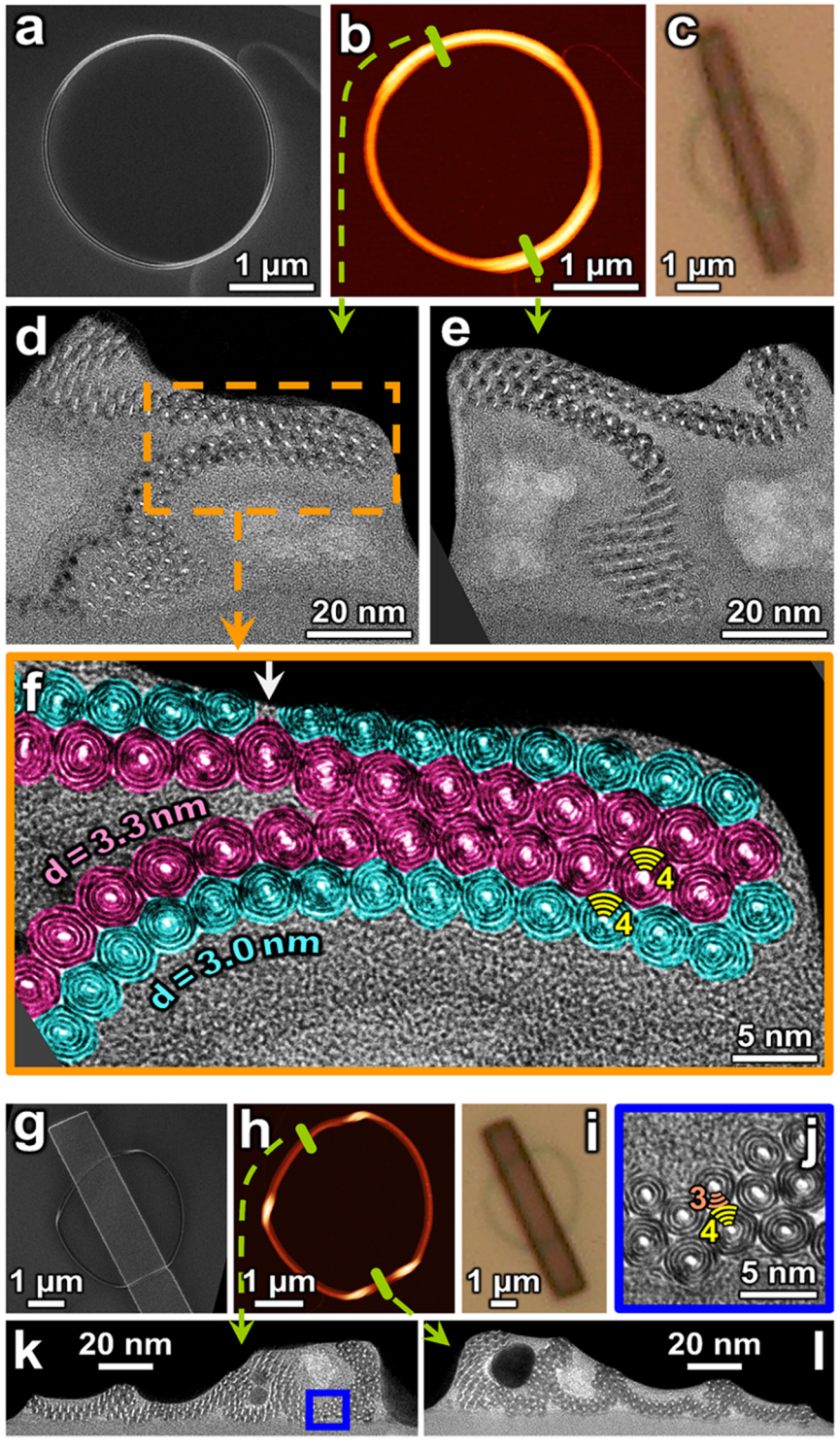

Figure 1. Structure of FWCNT coils. (a–f) Coil 1. (g–l) Coil 2. (a,g) SEM images. (b,h) AFM images. The lighter regions in b,h indicate twisted regions, reaching heights of 90 and 120 nm, respectively. The diagonal stripe in c, g, and i is due to lithography of the protection layer for lamella cutting. (c,i) Optical microscope images. (d,e,k,l) TEM images of the two sides of the cross-sectional lamella, showing 114 turns in Coil 1 and 163 turns in Coil 2. The locations from which the lamellae were taken are marked by the green lines in b and h. (f,j) Magnifications of d,k, respectively, which appear to show two types of FWCNTs in each coil: (f) Two four-wall CNTs with diameters 3.3 and 3.0 nm (standard deviations: ~0.17 nm). The turns are organized in a rippled two-layer raft configuration. The structure contains a "stacking fault" (marked by a white arrow at the top of subfigure f), possibly due to the mismatch in CNT diameters. The assignment of several turns to the 3.3 or 3.0 nm CNT is uncertain. (j) A TWCNT and a four-wall CNT. f and j are magnifications of the orange and blue rectangles in d and k, respectively.

postsynthesis sonication or were buried inside catalyst contaminations, comprised multiple CNTs in the same coil, and did not have free and accessible ends for electrical contacts.[12−14]

DOI: 10.1021/acs.nanolett.9b03977
Nano Lett. 2020, 20, 953−962

Micrometer-scale defect-free single-wall CNT (SWCNT) coils were recently demonstrated by our groups.[11] They were suggested to be formed by a nanometric variant of the coiling flexible rod mechanism,[7,9] nicknamed the "falling spaghetti" mechanism. This mechanism was also used to explain the formation of various other CNT geometries, including loops and serpentines.[16−20] According to it, the CNT first grows suspended above the substrate, then falls onto it. The final geometry is dictated by the CNT's stiffness and the local interplay between the downward and the forward components of its falling velocity. The downward component stems from van der Waals (vdW) attraction to the substrate and to previous loops (turns) of the coiled CNT. The forward component stems from the aerodynamic drag force applied by the gas flow. When the downward component dominates, the CNT self-organizes into a coil, similarly to the coiling of honey on a toast or shampoo on a hand.

Those previously reported coils comprised individual SWCNTs and were defect-free.[11] Yet, when tested as electromagnetic coils, they short-circuited due to current flowing between adjacent turns of the coils. This was explained by the perfectly matching chiralities between different turns of the coil (all made of the same nanotube), which pose no barrier for tunneling, in terms of conservation of crystal momentum. In contrast, few-wall CNTs [FWCNTs; e.g., double-wall CNT (DWCNT), triple-wall CNT (TWCNT), or four-wall CNT] are composed of coaxial CNT walls with different chiralities; therefore, in theory, tunneling between their walls is forbidden in terms of conservation of crystal momentum.[21,22] Having a sufficiently small interwall tunneling could make FWCNTs sheathed conductors that are suitable for the creation of electromagnetic coils. In practice, the interwall tunneling can be allowed by disorder causing momentum relaxation,[22] which is consistent with experimental observations.[23,24] In addition to conservation of crystal momentum, which may or may not effectively prevent interwall tunneling depending on the degree of disorder in the system, having a few walls instead of a single wall could enable additional sheathing mechanisms, such as depletion of charge carriers in the outer walls by gating,[25,26] or chemical functionalization of the outer wall.[27,28] In light of these considerations, FWCNT coils are promising candidates for electromagnetic coils where current flows along the inner wall(s) while the outer wall(s) acts as an insulating layer to prevent shorting between adjacent turns. For this purpose, FWCNT coils would need to have free ends for contacting and a low density of defects. However, FWCNT coils with such characteristics have not been produced yet. Moreover, the fact that SWCNTs were shown to spontaneously self-organize into defect-free coils does not necessarily imply that FWCNTs should do the same because the latter are significantly thicker and hence mechanically stiffer than the former.[29,30] For the same reason, neither is it obvious that, if they form, such FWCNT coils could have diameters in the same micrometer scale as the SWCNT coils. Therefore, demonstrating the formation of FWCNT coils is an important and nontrivial endeavor for both fundamental and practical purposes.

Besides their practical significance as potential candidates for electromagnetic coils, FWCNT coils could also be an attractive system for various fundamental studies, owing to their chiral and enantiomeric purity. A coil made of an individual FWCNT constitutes a homogeneous bundle of CNTs having precisely the same diameters and chiralities (including handedness). Naturally, this refers to walls of different CNT segments in the bundle, while the different walls composing the few-wall CNT have different diameters and chiralities by definition. Apart from a report on a few small DWCNT bundles that appeared to show identical chiralities from their electron diffraction,[31] virtually all bundles of FWCNTs contain a mixture of radii, chiralities, and handednesses, which adds complexity to studies of interwall[23,32−35] and intertube[36] interactions, transport,[37,38] and superconductivity.[39] For example, superconductivity was observed in bundles of DWCNTs, where a broadened superconducting transition was attributed to the mixed chirality in the bundles.[39] Using chirally pure bundles could, in future studies, lead to a much sharper superconducting transition, while the coil configuration could lead to the observation of persistent current through the coil. All of this makes FWCNT coils a potentially ideal system to study superconductivity as well as interwall and intertube coupling in CNTs.

Here, we demonstrate the formation of FWCNT coils and experimentally characterize them structurally, spectroscopically, and electrically, accompanied by fully atomistic molecular dynamics (MD) simulations of their formation mechanism. These CNT coils are found to be composed of DWCNTs, TWCNTs, and four-wall CNTs. The coils measure 2−4 μm in diameter, up to 120 nm in height, and comprise up to 163 turns. Raman spectroscopy found low defect densities, and fully atomistic molecular dynamics simulations support a coiling flexible rod[11] mechanism of formation of the FWCNT coils. The fact that these FWCNT coils have accessible ends for contacting enabled us to measure their electrical transport properties and to observe both metallic and semiconducting behaviors. Our results suggest that FWCNT coils are chirally and enantiomerically pure FWCNT bundles and are thus promising candidates for the future production of micrometer-size electromagnetic coils (beyond the scope of the present report), as well as for further fundamental studies of interwall and intertube interactions and superconductivity in CNTs.

We synthesized the FWCNTs by adapting a CVD (chemical vapor deposition) protocol that is known to yield mainly TWCNTs.[24] We grew the CNTs on Si/SiO_2 substrates using a catalyst of an $FeCl_3$ drop or stripes of evaporated Fe (see the Methods section). The CNTs' self-organization on the silicon wafers facilitates their integration into devices by traditional lithographic methods, as we demonstrate later on. After synthesis, we imaged the samples using a SEM (scanning electron microscope) and found tens of coils per sample (Figure 1a,g), as well as other CNT geometries, including straight segments, serpentines, and loops (Supporting Figure S1a). The coil diameters were typically 2−4 μm, although diameters as small as 1 μm and as large as 13 μm were also observed (all much smaller than the persistence length, which is hundreds of micrometers; see the Supporting Information for the calculation[40]). The uncoiled CNT segments connected to the coil are called "tails" (or "free ends," seen in the top-right and bottom of Figure 1a and in Supporting Figure S3a). The number of FWCNT coils characterized using each experimental method is provided in the Supporting Information.

AFM (atomic force microscope) imaging enables a rough estimation of the number of turns in a coil (Figure 1b,h). By comparing the tail heights (typically 2−5 nm) to the coil heights (bundle heights, up to 120 nm, Figure 1h) and widths (tens of nanometers, Figure 1a,g), we could roughly estimate

DOI: 10.1021/acs.nanolett.9b03977
Nano Lett. 2020, 20, 953−962

that the coils have several tens of turns per coil. Some of our coils comprise enough turns to be observable even in a regular optical microscope, although the tails are imperceptible (Figure 1c,i; The diagonal stripe in Figure 1c,g,i is of lithography). The AFM images also show that some parts of the coil are significantly taller than the rest of the coil (bright regions in Figure 1h). These regions are identified as twisted regions, where the coil's cross section twists on the substrate.[11] Similar twisting is seen in many of our coils (Figures 1a,b,g,h and 2b,c and Supporting Figures S2a,b, S3c,d and S5c,d) and in other coiled CNTs,[11−13] and is further discussed in the Supporting Information.

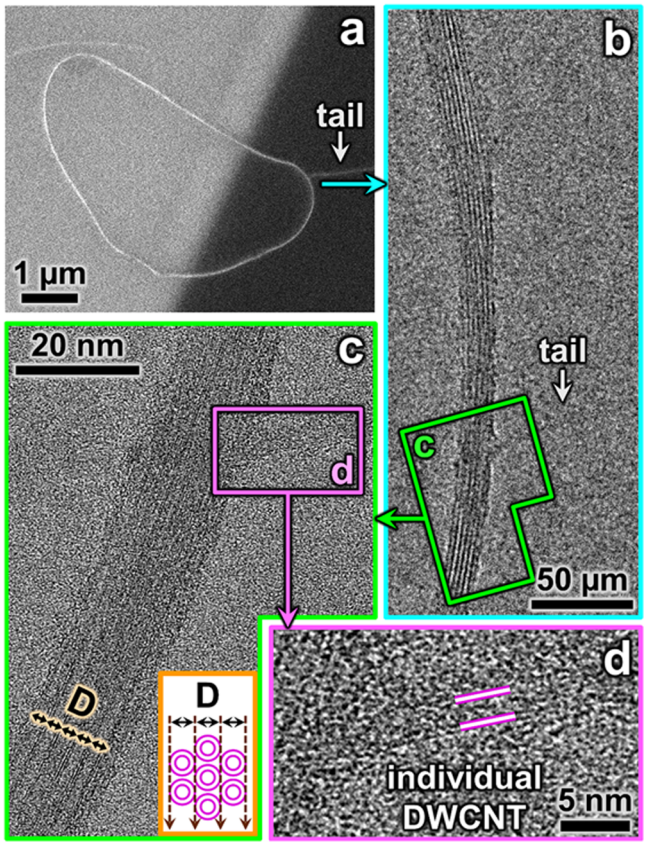

Figure 2. Top-view TEM imaging of a FWCNT coil (Coil 3). (a) SEM image of a coil after it was transferred onto a TEM grid window. (b) Medium-magnification and (c) high-magnification TEM image of the tail and the coil, showing fringes. The fringes at the bottom of c can be interpreted as a periodicity of a hexagonal packing of DWCNTs. Inset: illustration of the cross section of a hexagonal packing of DWCNTs and its periodicity. (d) Magnification of the tail.

In order to count precisely the number of turns in each coil and the number of walls in each CNT, as well as to study the coils' structure in more detail, we imaged 10 coils using either top-view TEM (transmission electron microscope; five coils) or cross-sectional-view TEM (five coils). Eight coils were composed of FWCNTs, and the other two were composed of SWCNTs.

Imaging coils using cross-sectional TEM is enabled by cutting each coil into a thin lamella using a focused ion beam (FIB). Figure 1d,e,k,l shows TEM images of the cross sections of the coils in Figure 1b,h. These cross sections of Coils 1 and 2 comprise 114 and 163 turns, respectively, organized in a rippled two-layer configuration reminiscent of a hexagonal packing. The vertical raft structure appears folded and rippled, with a width of two CNTs. Overall, there is a strong agreement between our SEM, AFM, cross-sectional TEM, and top-view TEM images. There is also an agreement with other coiled SWCNTs,[11] DWCNTs,[12] and TWCNTs,[13] apart for the raft structures. Therefore, we infer that the basic structural features of the lamellae, including the raft structure and its partial collapse onto the substrate, were also present in the pristine coils before the process.

Interestingly, two types of turns of FWCNTs were observed for each of the two coils: Coil 1 appears to comprise two four-wall CNTs with two different diameters (3.3 and 3.0 nm) coiled together (Figure 1f), and Coil 2 comprised a four-wall CNT and a TWCNT coiled together (Figure 1j). Turns of the two CNTs were observed side-by-side throughout the cross sections of these coils (see also Supporting Figure S4). The existence of two CNTs per coil in Coils 1 and 2 possibly facilitated these high-aspect-ratio, two-CNT-thick, ribbon-like structures, which were not reported in other coiled CNT structures.[11]

To study the morphology of the coils and their tails in a nondestructive way and to corroborate the cross-sectional TEM results, we imaged them by top-view TEM (Figure 2 and Supporting Figure S5). To this end, we successfully transferred complete coils onto TEM grids, using a polymer.[41] This demonstrates that the coils can be transferred to a substrate transparent to electrons and light, with no evident damage, which could be useful for future applications. Fringes in the TEM images of Coil 3 indicate that it has an ordered structure (Figure 2b,c). The fringe pattern can be interpreted as resulting from a periodicity of a hexagonally packed bundle of DWCNTs (inset in Figure 2c).[12,13] This is supported by the partial hexagonal packing seen in the cross-sectional lamellae (Figure 1f,j) and in other coiled CNTs.[11−13] Indeed, the tail itself is identified as an individual DWCNT (Figure 2d). The fringe patterns in the coils appear only in certain regions, suggesting that the coils twist into and out of the TEM zone axis (Figure 2b,c and Supporting Figure S5c,d), as discussed earlier and in the Supporting Information.[11−13]

We used confocal resonant Raman spectroscopy with multiple excitation wavelengths to study the structure of the CNTs in our coils and assess their density of defects. Figure 3a,b,e,f,i,j show SEM images and lateral mappings of the Raman G mode intensity of Coils 4−6, respectively. The existence of one and two maxima (lobes) in the Raman intensity maps stems from the polarization of the exciting laser (parallel to the figure's horizontal axis) and the shapes of the coils (see Supporting Information for further details).[42]

The radial breathing mode (RBM) region of the Raman spectra is shown in Figure 3c,g,k. Multiple excitation wavelengths are needed to probe the different walls of a FWCNT. Under excitation energies from 1.58 to 2.54 eV, two RBMs were detected in both Coils 4 and 5, and three RBMs were detected in Coil 6. These RBM frequencies correspond to wall diameters of 0.9@1.6, 1.0@1.7, and 1.8@2.5@3.1 nm, in Coils 4−6, respectively (denoted as inner-wall@outer-wall; see the Methods section for the calculation).[42,43] The G mode of a particular wall is not always accompanied by that wall's RBM, due to the narrower excitation energy window of the latter mode.[44] Regarding the G mode, splitting of its G^+ component (longitudinal phonon for semiconducting walls) is seen (Figure 3d,h,l). This splitting is attributed to interwall interactions within one FWCNT, where the G^+ mode of the

DOI: 10.1021/acs.nanolett.9b03977
Nano Lett. 2020, 20, 953−962

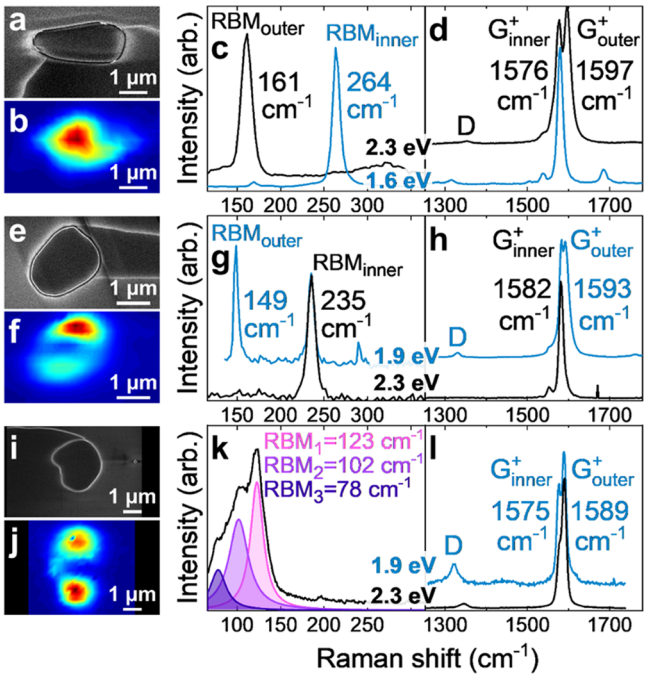

Figure 3. Raman spectroscopy of FWCNT coils. (a–d) Coil 4. (e–h) Coil 5. (i–l) Coil 6. (a,e,i) SEM images. (b,f,j) G mode mapping (step size: 300 nm). (c,g,k) RBM regions of the Raman spectra, indicating: two walls with diameters 0.9@1.6 nm (subfigure c, Coil 4), two walls with diameters 1.0@1.7 nm (subfigure g, Coil 5), and three walls with diameters 1.8@2.5@3.1 nm (subfigure k, Coil 6). (d,h,l) G and D mode regions of the Raman spectra showing splitting of the G^+ modes of the inner and outer walls, as well as low defect (D) peaks.

inner (outer) wall shifts to a smaller (higher) frequency relative to the position in an isolated single-wall CNT.[35,45,46] This indicates that the Raman signals belong to the walls of a FWCNT, rather than to separate SWCNTs.[35,45] Overall, we imaged 14 coils by Raman spectroscopy, for 7 of which we could detect a G^+ mode splitting.

On the basis of the intensity ratio of the G^+ peaks of the coils and their tails (G^+_{coil}/G^+_{tail}), we estimate the number of turns in Coils 4–6 to be at least 17, 60, and 26, respectively. The combination of the shape of the G mode, the energy of the RBM, and the resonance energy of the wall suggests that all the walls shown in Figure 3 are semiconducting.[42] Nevertheless, we were also able to detect metallic walls by Raman spectroscopy (Supporting Figure S6).

The Raman spectra of the coils were compared to those of the tails (Supporting Figure S7). Crystal disorder was assessed using the disorder-induced D mode around 1350 cm^{-1}.[42] The D/G intensity ratio in the tails was very small (<0.01), reflecting excellent crystallinity and negligible defect densities. This was measured for both straight and curved tail segments. The D/G intensity ratios in the coils were sometimes below 0.01 but reached up to 0.10 (Figure 3d,h,l and Supporting Table 1; under 1.9 eV, Coil 6 had a D/G ratio of 0.20). Although this was higher than in the tails, it remains a very small D/G ratio for CNTs. Generally, the appearance of the D mode is related to disorder in the sample (e.g., structural defects, broken translational symmetry, kinks, and so on).[42,47] To better understand the origin of the slight increase in D mode intensity, we first consider the coils of SWCNTs. They had a negligibly small D mode[11] and so did SWCNT serpentines at both originally curved and manually strained regions.[48,49] Individual SWCNTs (or bundles of aligned, identical CNTs) have stringent conditions for the activation of the D mode, because they conserve rotational in addition to linear momentum.[50] In contrast, SWCNT bundles that are composed of different CNTs have higher D modes than individual CNTs.[42] The FWCNT coils presented here often contain more than one FWCNT, which affects the translational symmetry and offers more partners for the elastic, defect-related scattering necessary for the activation of the D mode. In addition, the coils are often twisted, which lifts the rotational symmetry.[50] While we cannot rule out the formation of structural defects within the coils, no defects were found in the SWCNT coils, the overall curvature in our coils is low, and our MD simulations predicted no formation of defects even in highly curved regions. We suggest that a small increase in D mode intensity upon coil formation is an intrinsic fingerprint of combining several FWCNT segments in a twisted manner.

Another interesting phenomenon in the spectra is a red shift in the G^+ mode frequency of Coils 5 and 6 (4.5 and 8 cm^{-1}, respectively), with respect to their tails (Supporting Figure S7). This shift could result from strain in the coils, possibly due to twisting and intertube interactions. Such a shift was seen in SWCNT serpentines (where it was suggested to stem from interaction with the substrate)[49] but not in SWCNT coils,[11] possibly because of differences in the exact packing of the coils and the lower stiffness of SWCNTs. Overall, our Raman results demonstrate that chirally pure FWCNT coils are an important model system for further studies on bundling effects in FWCNTs, which could be otherwise obfuscated by the heterogeneous chiralities in regular bundles.

The formation mechanism of the coils was studied using fully atomistic molecular dynamics (MD) simulations. One of the aims of these simulations was to test whether the coils could form by the coiling flexible rod mechanism, similarly to the defect-free SWCNT coils,[11] despite the higher stiffness of FWCNTs (Supporting Figure S12).[29,30] The coiling of an individual DWCNT was modeled at temperatures of 10 and 1270 K using 600 000 atoms over 20 000 000 time steps (Figure 4a and Supporting Movies S1,2,4,5). It showed that once the first turn of the coil is formed, the rest of the DWCNT immediately continues to coil by attaching to the previous turns. Specifically, despite the elastic energy cost of bending the DWCNT, the attractive vdW force between CNT-turns renders the formation of additional turns (i.e., further coiling) much more favorable energetically (Figure 4b). For this reason, the coiled configuration is even more energetically favorable than the straight one (Supporting Figure S12). While both the coiling of a SWCNT[11] and of a DWCNT are favorable energetically, the coiling of a DWCNT is slower, as the energy gain per length of CNT is smaller and the inertia is higher (Supporting Figure S9). Analysis of stress distribution during coil formation reveals that, while the suspended bent CNT segment near the coil exhibits a relatively high stress, this stress quickly decreases after the segment deposits on the coil (Supporting Movies S3 and S6). One exception is regions where the coil twists, since torsion introduces additional stress. Regarding a pentagon–heptagon defect, which generally can occur due to bending strain, its formation rate is negligible under the maximal bending strain in the coiled structure, under the conditions found in our simulations.[51] In addition, we performed reactive simulations of these highly curved loops using the AIREBO reactive force field[52] and found no formation of defects (Supporting Figure S13). Detailed

DOI: 10.1021/acs.nanolett.9b03977
Nano Lett. 2020, 20, 953–962

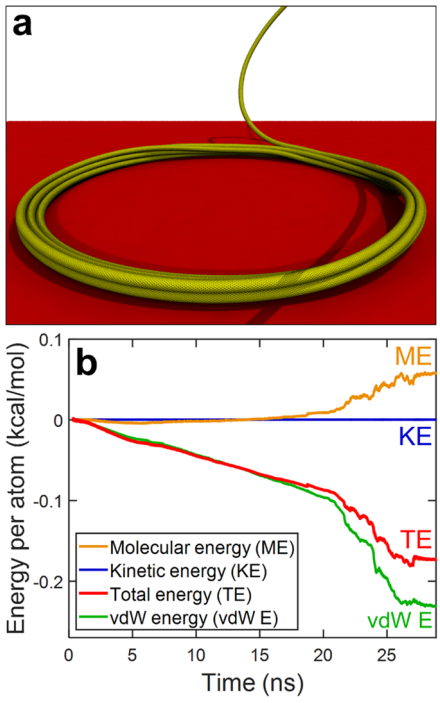

Figure 4. Molecular dynamics (MD) simulation of the formation of a DWCNT coil. (a) Representative MD snapshot of the coil formation (see the Supporting Movies). (b) Evolution of the different energy components during coil formation. The results are for a temperature of 10 K (qualitatively similar results for 1270 K are presented in Supporting Figure S10).

discussion, results, and methods are presented in the Supporting Information.

On the basis of these simulations, we can conclude that the FWCNT coils are formed according to a variant of the general coiling flexible rod mechanism[7,9] termed the falling spaghetti mechanism:[11,19] A CNT grows in the flying mode, suspended above the substrate and then falls onto the substrate and coils, as described in the introduction. This conclusion is supported by the similarities with the defect-free SWCNT coils (grown in the same CVD system and having comparable results of SEM, AFM, TEM, Raman spectroscopy, and MD simulations).[11,19] Importantly, the CNT does coil despite the higher stiffness of FWCNTs (Supporting Figure S12).[29,30] Notably, some of the coils presented here comprise turns of more than one CNT (Figure 1 and Supporting Figures S3f,h, S5, and S14). We suggest that they were formed according to the same mechanism, some by coiling of a bundle of several CNTs, and some by sequential coiling of several CNTs, one after the other (see the relevant discussion in the Supporting Information). The high-aspect-ratio, raft configuration of the coils further supports this mechanism, suggesting that the CNT falls and piles up preferentially on the upper part of the coil. This phenomenon has been studied in the macroscopic coiling of flexible rods and viscous jets, such as when pouring honey on a toast or shampoo on a hand.[7]

The electrical properties of the coils and their tails were studied in a field-effect transistor setup. Source and drain electrodes were evaporated onto the outer wall of the CNTs. We found coils showing *p*-type semiconducting (Coil 7, Figure 5a,b) and metallic (Coil 8, Figure 5c,d) behaviors. On the basis of its response to gating, Coil 7 is likely composed of a semiconducting outer wall(s).[25,53] It seems to have short-

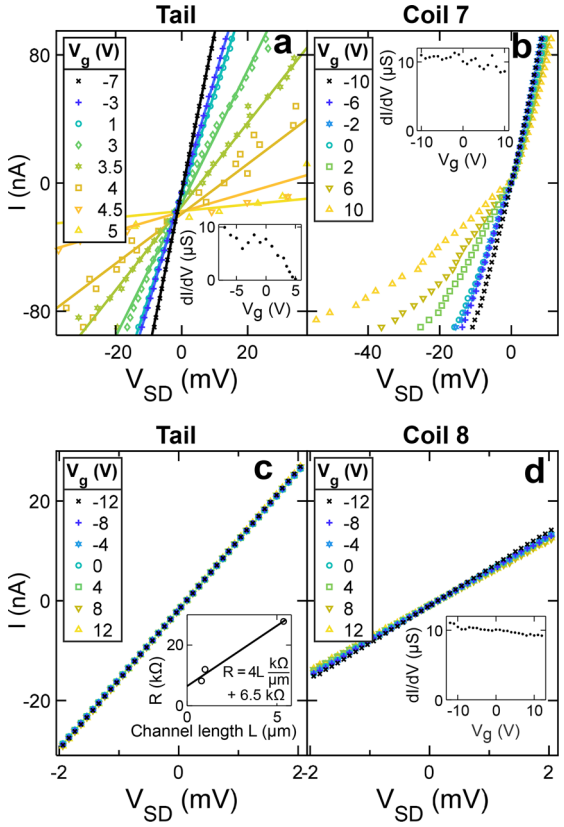

Figure 5. Electrical properties of FWCNT coils. (a,b) Coil 7 (three turns of a TWCNT). (c,d) Coil 8 (an estimated 13 turns of a CNT with a diameter of 3.5 nm and an estimated 1−6 walls; see the Supporting Information). (a−d) Current (I) vs source−drain voltage (V_{SD}), at various gate voltages (V_g, in the legends, in volts), for: (a,c) the tails and (b,d) the coils. The insets in a,b,d show the average differential conductance (dI/dV_{SD}) vs V_g (in a and c, averaged over all V_{SD}, and in b, averaged over positive V_{SD} values). The inset in c shows the result of the transmission-line measurements: two probe resistance (R) vs tail segment length (L). Solid lines are linear fits. See Supporting Figures S15 and S16 for additional details.

circuited, as is apparent when comparing its resistance (Figure 5a) to the resistance of its tail (Figure 5b), while Coil 8 showed a higher resistivity than its tail (Figure 5c,d), which could be attributed to partial short-circuiting or to defects in the CNT. More details are provided in the Supporting Information.

As discussed in the introduction, FWCNT coils are especially attractive for their potential applications as induction coils. The short-circuiting between turns that is observed in the FWCNT coils that we tested may be expected because contacts were laid down onto the outer walls, which are commensurate with one another, as in the case of SWCNT coils. A possible future method to prevent short-circuiting, which is possible in FWCNTs and not in SWCNTs, is to inject the current selectively into the inner wall of a FWCNT coil. This could be done by exposing the inner wall using electrical breakdown,[54] chemical etching,[55] or mechanical pulling.[56] Provided a large enough interwall resistivity,[21,23] the outer wall(s) would act as sheathing, while current would flow through the inner wall. Moreover, other FWCNT coils that have a semiconducting outer wall(s) and a metallic inner wall(s) could possibly avoid short-circuiting, particularly when tested at low temperatures.[23,25,57] Positively gating the *p*-type

DOI: 10.1021/acs.nanolett.9b03977
Nano Lett. 2020, 20, 953−962

semiconducting outer wall(s), thereby depleting it from charge carriers, could further turn it into sheathing. Previous works suggested that near the source and drain electrodes, gating is less effective, allowing current to pass from the electrodes, through the outer wall, to the inner wall.[25,26,53] Generally, ~22% of DWCNTs are expected to have the M@S (i.e., metallic inside semiconducting) electronic configuration and ~15% of TWCNTs are expected to have the M@S@S configuration.[25] Short-circuiting might further be avoided by using a FWCNT with more walls for sheathing and by selectively functionalizing the outer wall.[27,28] If an outer wall(s) can indeed provide sufficiently good insulation, the coil could act as an electromagnetic coil. These experiments are very interesting for future studies, but also laborious and beyond the scope of the present report.

One can roughly estimate that a coil similar to the one shown in Figure 1a, if effectively sheathed, would have an inductance of up to 40 nH with an air core (see Supporting Information for the calculations). For comparison, this inductance would be 1 order of magnitude higher than that of a 200 μm size microfabricated solenoid (which is 2 orders of magnitude larger in size than the FWCNT coils),[58] and only 1 order of magnitude lower than the inductance of a millimeter-scale microfabricated air-core inductor (which is 3 orders of magnitude larger in size than the FWCNT coil).[59] Supposing a current-carrying capacity of 25 μA,[60] such a coil could induce a magnetic flux density **B** of 1.3 mT at its core (i.e., comparable to that of a refrigerator magnet). The inductance and flux density of a FWCNT could be significantly increased by introducing a microfabricated ferromagnetic core inside the coil. Therefore, sheathed FWCNT coils could be extremely powerful miniature electromagnets and inductors.

In summary, we have demonstrated the formation of micrometer-scale few-wall carbon nanotube (FWCNT) coils, and characterized their structural and electrical properties using optical microscopy, SEM, AFM, cross-sectional TEM, top-view TEM, Raman spectroscopy, MD simulations, and electrical transport measurements. We found compact coils composed of DWCNTs, TWCNTs, and four-wall CNTs with low defect densities. Some of them are composed of an individual FWCNT, while the others are composed of thin bundles of several FWCNTs. We suggest that the FWCNT coils self-organize on their growth substrate according to the coiling flexible rod mechanism, similarly to defect-free SWCNT coils and poured honey.[7,11,19] These results generalize the coiling flexible rod mechanism to the stiffer FWCNTs and CNT bundles, suggesting that the mechanism is applicable to other flexible 1D nanomaterials. FWCNT coils are an important addition to the known repertoire of available CNT structures for nanoscience and nanotechnology. These FWCNT coils have accessible tails, which enable electrical contacts. When measured electrically, the coils showed either metallic or semiconducting behavior. The coils tested probably short-circuited, as may be expected when contacts are made to their outer walls. Nevertheless, we believe that under the conditions that we proposed (e.g., a semiconducting outer wall(s) and a metallic inner wall(s), gating, and possibly low temperatures or selectively contacting the inner wall), FWCNT coils could avoid short-circuiting and lead to FWCNT induction coils. Even if interwall tunneling were not completely avoided but quantitatively reduced, this would increase the effective number of turns made by the current around the coil and thus significantly increase its inductance with respect to that of a fully short-circuited coil.

Such sheathed induction coils (even if only partially sheathed) could be the basis for a variety of micrometer-scale inductive devices, such as electromagnets, inductors, transformers, and motors. Miniature electromagnets could be particularly useful for on-chip nuclear magnetic resonance (NMR) in microfluidic systems.[61] FWCNT coils are also interesting from a fundamental point of view because they consist of chirally and enantiomerically pure FWCNT bundles. These clean bundles are, thus, an ideal system to investigate intertube and interwall coupling effects in CNTs,[35,38] as well as other interesting phenomena such as superconductivity in CNTs.[39] Superconductivity was observed in bundles of DWCNTs, where a broadened superconducting transition was attributed to the mixed chirality in the bundles.[39] Using chirally pure bundles could lead to a much sharper superconducting transition. Moreover, the coil configuration of these bundles could lead to the generation of a persistent current. All of this makes chirally pure FWCNT coils with accessible ends, first demonstrated here, a new and attractive nanostructure for fundamental studies and potential applications.

METHODS

See also the Supporting Information for additional details.

Synthesis of FWCNT Coils. A catalyst of ferric chloride hexahydrate solution[24] or stripes of evaporated Fe (ref 11) were deposited on Si/SiO_2 substrates. A synthesis method based on chemical vapor deposition was adjusted to produce mostly TWCNTs with minimal SWCNTs (temperature: 1000 °C; gases: CH_4/H_2 ratio of 1/5; flow rate: 54 cm^3/min at ambient conditions; duration: 30−40 min).[24] For comparison, our growth method differs from that of the SWCNT coils in ref 11 in that there, the catalyst was always stripes of evaporated Fe, and the gases were 60:40:0.2 $Ar:H_2:C_2H_4$ at a total flow rate of 70−2000 cm^3/min. The same system was used.

Imaging. Standard photolithography, electron beam lithography, and electron beam evaporation were used to deposit alignment marks and electrical contacts. Optical microscopy, SEM, AFM, and TEM were used to image the coils. Cross-sectional TEM imaging was performed as in ref 11. For top-view TEM imaging, complete coils were transferred onto TEM grids by adapting the method in ref 41 for TEM grids.

Raman Characterization. Raman spectra were acquired with the Xplora and T64000 Horiba spectrometers, with 1.58, 1.72, 1.9, 2.2, 2.33, and 2.54 eV laser excitation sources. RBM frequencies were used to estimate the diameters (d) of the FWCNT walls using the following relation: $d = 227/(\omega_{RBM} - \Delta_{FW-SW})$.[62] Δ_{FW-SW} reflects the difference between the RBM shift of that wall in a FWCNT and in the corresponding SWCNT[42,43] and can vary from 2 to 20 cm^{-1}.[62]

Electrical Characterization. Field-effect transistors were produced from the coils and measured in a method similar to that of ref 11, and see the Supporting Information for more details. A low-pass filter was used for Coil 8, and the filter's resistance (43.8 kΩ) was excluded from the reported resistances and differential conductances but not from the reported voltages. Throughout the Communication, error ranges denote standard deviations unless otherwise indicated.

Molecular Dynamics (MD). The simulations were carried out using the CHARMM[63] and AIREBO[52] force fields, as

DOI: 10.1021/acs.nanolett.9b03977
Nano Lett. 2020, 20, 953−962

implemented in the LAMMPS package.[64] More details and results are available in the Supporting Information.

■ ASSOCIATED CONTENT

Supporting Information

The Supporting Information is available free of charge at https://pubs.acs.org/doi/10.1021/acs.nanolett.9b03977.

Movie of MD simulation of the formation of a DWCNT coil at 10 K, zoomed-in view (AVI)

Movie of MD simulation of the formation of a DWCNT coil at 10 K, zoomed-out view (AVI)

Movie of MD simulation of the formation of a DWCNT coil at 10 K, stress analysis (AVI)

Movie of MD simulation of the formation of a DWCNT coil at 1270 K, zoomed-in view (AVI)

Movie of MD simulation of the formation of a DWCNT coil at 1270 K, zoomed-out view (AVI)

Movie of MD simulation of the formation of a DWCNT coil at 1270 K, stress analysis (AVI)

(1) Discussion on the expected interwall resistivity; (2) Additional Figure: Low-magnification view of a sample; (3) Additional discussion on coil morphology, including twisting; (4) Additional discussion on the top-view TEM imaging; (5) Additional Raman measurements and discussion; (6) Summary statistics of the structural analysis; (7) Estimation of the persistence length; (8) Additional molecular dynamics (MD) simulations; (9) Additional discussion on the formation of coils of bundles; (10) Additional electrical measurements; and (11) Detailed methods (PDF)

■ AUTHOR INFORMATION

Corresponding Author

*E-mail: ernesto.joselevich@weizmann.ac.il.

ORCID

Dekel Nakar: 0000-0003-3814-7115
Georgy Gordeev: 0000-0002-3273-2105
Leonardo D. Machado: 0000-0003-1221-4228
Eliezer F. Oliveira: 0000-0002-7161-8217
Patryk Kusch: 0000-0001-9180-786X
Douglas S. Galvão: 0000-0003-0145-8358
Ernesto Joselevich: 0000-0002-9919-0734

Author Contributions

The manuscript was written through the contributions of all authors. All authors have given approval to the final version of the manuscript.

Funding

E.J. acknowledges support from the European Research Council (ERC Advanced Grant number 338849), and the Minerva Stiftung (grant number 713215). G.G, P.K, and S.R acknowledge the German Research Foundation (DFG via SFB 658, subproject A6). L.D.M., E.F.O., and D.S.G. are supported by the Brazilian agencies CNPq, CAPES, and FAPESP (grant numbers 2013/08293-7 and 2016/18499-0). A.J is supported by the Humboldt Foundation and the Brazilian agencies CNPq (grant number 429165/2018-8) and CAPES (grant number 88881.198744/2018-01).

Notes

The authors declare no competing financial interest.

■ ACKNOWLEDGMENTS

D.N. and E.J. thank Nitzan Shadmi for helpful discussions. We thank Lothar Houben for help with TEM imaging. E.J. holds the Drake Family Professorial Chair of Nanotechnology and acknowledges support from the European Research Council (ERC Advanced Grant number 338849), and the Minerva Stiftung (grant number 713215). This research was also partly supported by the Helen and Martin Kimmel Center for Nanoscale Science, the Moscowitz Center for Nano and Bio-Nano Imaging, and the Perlman Family Foundation. D.N. acknowledges support from the Feinberg Graduate School. G.G., P.K., and S.R. acknowledge the German Research Foundation (DFG via SFB 658, subproject A6). L.D.M., E.F.O., and D.S.G. are supported by the Brazilian agencies CNPq, CAPES, and FAPESP (grant numbers 2013/08293-7 and 2016/18499-0). D.S.G, L.D.M., and E.F.O would like to thank the Center for Computational Engineering and Sciences at Unicamp for financial and computational support. LDM would also like to acknowledge the support of the High Performance Computing Center at UFRN (NPAD/UFRN). A.J. acknowledges support from the Humboldt Foundation and the Brazilian agencies CNPq (grant number 429165/2018-8) and CAPES (grant number 88881.198744/2018-01).

■ ABBREVIATIONS

AFM, atomic force microscope
CNT, carbon nanotube
CVD, chemical vapor deposition
DWCNT, double-wall CNT
FIB, focused ion beam
FWCNT, few-wall CNT
MD, molecular dynamics
MWCNT, multiwall CNT
SEM, scanning electron microscope
SWCNT, single-wall CNT
TEM, transmission electron microscope
TWCNT, triple-wall CNT
vdW, van der Waals

■ REFERENCES

(1) Rao, R.; Pint, C. L.; Islam, A. E.; Weatherup, R. S.; Hofmann, S.; Meshot, E. R.; Wu, F.; Zhou, C.; Dee, N.; Amama, P. B.; et al. Carbon Nanotubes and Related Nanomaterials: Critical Advances and Challenges for Synthesis toward Mainstream Commercial Applications. *ACS Nano* **2018**, *12* (12), 11756−11784.

(2) Tans, S. J.; Verschueren, A. R. M.; Dekker, C. Room-Temperature Transistor Based on a Single Carbon Nanotube. *Nature* **1998**, *393* (6680), 49−52.

(3) Yao, Z.; Postma, H. W. C.; Balents, L.; Dekker, C. Carbon Nanotube Intramolecular Junctions. *Nature* **1999**, *402* (6759), 273−276.

(4) Snow, E. S. Chemical Detection with a Single-Walled Carbon Nanotube Capacitor. *Science* **2005**, *307* (5717), 1942−1945.

(5) Shulaker, M. M.; Hills, G.; Patil, N.; Wei, H.; Chen, H.-Y.; Wong, H.-S. P.; Mitra, S. Carbon Nanotube Computer. *Nature* **2013**, *501* (7468), 526−530.

(6) Habibi, M.; Ribe, N. M.; Bonn, D. Coiling of Elastic Ropes. *Phys. Rev. Lett.* **2007**, *99* (15), 154302.

(7) Ribe, N. M.; Habibi, M.; Bonn, D. Liquid Rope Coiling. *Annu. Rev. Fluid Mech.* **2012**, *44* (1), 249−266.

(8) Smarter Every Day; Sandlin, D. Amazing Honey Coiling High Speed Video! - Smarter Every Day 53 − YouTube. https://www.youtube.com/watch?v=zz5lGkDdk78 (accessed Jul 15, 2019).

DOI: 10.1021/acs.nanolett.9b03977
Nano Lett. 2020, 20, 953−962

(9) Jawed, M. K.; Da, F.; Joo, J.; Grinspun, E.; Reis, P. M. Coiling of Elastic Rods on Rigid Substrates. *Proc. Natl. Acad. Sci. U. S. A.* **2014**, *111* (41), 14663−14668.
(10) Eickbush, T. H.; Moudrianakis, E. N. The Compaction of DNA Helices into Either Continuous Supercoils or Folded-Fiber Rods and Toroids. *Cell* **1978**, *13* (2), 295−306.
(11) Shadmi, N.; Kremen, A.; Frenkel, Y.; Lapin, Z. J.; Machado, L. D.; Legoas, S. B.; Bitton, O.; Rechav, K.; Popovitz-Biro, R.; Galvão, D. S.; et al. Defect-Free Carbon Nanotube Coils. *Nano Lett.* **2016**, *16* (4), 2152−2158.
(12) Colomer, J.-F.; Henrard, L.; Flahaut, E.; Van Tendeloo, G.; Lucas, A. A.; Lambin, P. Rings of Double-Walled Carbon Nanotube Bundles. *Nano Lett.* **2003**, *3* (5), 685−689.
(13) Yu, H.; Zhang, Q.; Luo, G.; Wei, F. Rings of Triple-Walled Carbon Nanotube Bundles. *Appl. Phys. Lett.* **2006**, *89* (22), 223106.
(14) Liu, L.; Zhao, J. Toroidal and Coiled Carbon Nanotubes. In *Syntheses and Applications of Carbon Nanotubes and Their Composites*; Suzuki, S., Ed.; InTech, 2013; pp 257−281. DOI: 10.5772/51125.
(15) Akagi, K.; Tamura, R.; Tsukada, M.; Itoh, S.; Ihara, S. Electronic Structure of Helically Coiled Cage of Graphitic Carbon. *Phys. Rev. Lett.* **1995**, *74* (12), 2307−2310.
(16) Geblinger, N.; Ismach, A.; Joselevich, E. Self-Organized Nanotube Serpentines. *Nat. Nanotechnol.* **2008**, *3* (4), 195−200.
(17) Shadmi, N.; Geblinger, N.; Ismach, A.; Joselevich, E. Formation of Ordered vs Disordered Carbon Nanotube Serpentines on Anisotropic vs Isotropic Substrates. *J. Phys. Chem. C* **2014**, *118* (25), 14044−14050.
(18) Machado, L. D.; Legoas, S. B.; Soares, J. S.; Shadmi, N.; Jorio, A.; Joselevich, E.; Galvão, D. S. Dynamics of the Formation of Carbon Nanotube Serpentines. *Phys. Rev. Lett.* **2013**, *110* (10), 105502.
(19) Jawed, M. K.; Hadjiconstantinou, N. G.; Parks, D. M.; Reis, P. M. Patterns of Carbon Nanotubes by Flow-Directed Deposition on Substrates with Architectured Topographies. *Nano Lett.* **2018**, *18* (3), 1660−1667.
(20) Joselevich, E. Self-Organized Growth of Complex Nanotube Patterns on Crystal Surfaces. *Nano Res.* **2009**, *2* (10), 743−754.
(21) Yoon, Y.-G.; Delaney, P.; Louie, S. G. Quantum Conductance of Multiwall Carbon Nanotubes. *Phys. Rev. B: Condens. Matter Mater. Phys.* **2002**, *66* (7), 073407.
(22) Tunney, M. A.; Cooper, N. R. Effects of Disorder and Momentum Relaxation on the Intertube Transport of Incommensurate Carbon Nanotube Ropes and Multiwall Nanotubes. *Phys. Rev. B: Condens. Matter Mater. Phys.* **2006**, *74* (7), 075406.
(23) Bourlon, B.; Miko, C.; Forró, L.; Glattli, D. C.; Bachtold, A. Determination of the Intershell Conductance in Multiwalled Carbon Nanotubes. *Phys. Rev. Lett.* **2004**, *93* (17), 176806.
(24) Wen, Q.; Qian, W.; Nie, J.; Cao, A.; Ning, G.; Wang, Y.; Hu, L.; Zhang, Q.; Huang, J.; Wei, F. 100 Mm Long, Semiconducting Triple-Walled Carbon Nanotubes. *Adv. Mater.* **2010**, *22* (16), 1867−1871.
(25) Wang, S.; Liang, X. L.; Chen, Q.; Zhang, Z. Y.; Peng, L.-M. Field-Effect Characteristics and Screening in Double-Walled Carbon Nanotube Field-Effect Transistors. *J. Phys. Chem. B* **2005**, *109* (37), 17361−17365.
(26) Morimoto, T.; Kuno, A.; Yajima, S.; Ishibashi, K.; Tsuchiya, K.; Yajima, H. Effective Energy Gap of the Double-Walled Carbon Nanotubes with Field Effect Transistors Ambipolar Characteristics. *Appl. Phys. Lett.* **2012**, *100* (4), 043107.
(27) Brozena, A. H.; Moskowitz, J.; Shao, B.; Deng, S.; Liao, H.; Gaskell, K. J.; Wang, Y. Outer Wall Selectively Oxidized, Water-Soluble Double-Walled Carbon Nanotubes. *J. Am. Chem. Soc.* **2010**, *132* (11), 3932−3938.
(28) Piao, Y.; Chen, C.-F. F.; Green, A. A.; Kwon, H.; Hersam, M. C.; Lee, C. S.; Schatz, G. C.; Wang, Y. Optical and Electrical Properties of Inner Tubes in Outer Wall-Selectively Functionalized Double-Wall Carbon Nanotubes. *J. Phys. Chem. Lett.* **2011**, *2* (13), 1577−1582.
(29) Zhao, J.; Lu, L.; Rabczuk, T. Binding Energy and Mechanical Stability of Single- and Multi-Walled Carbon Nanotube Serpentines. *J. Chem. Phys.* **2014**, *140* (20), 204704.
(30) Wong, E. W.; Sheehan, P. E.; Lieber, C. M. Nanobeam Mechanics: Elasticity, Strength, and Toughness of Nanorods and Nanotubes. *Science* **1997**, *277* (5334), 1971−1975.
(31) Colomer, J.-F.; Henrard, L.; Launois, P.; Van Tendeloo, G.; Lucas, a a.; Lambin, P. Bundles of Identical Double-Walled Carbon Nanotubes. *Chem. Commun.* **2004**, *132* (22), 2592.
(32) Liu, K.; Jin, C.; Hong, X.; Kim, J.; Zettl, A.; Wang, E.; Wang, F. Van Der Waals-Coupled Electronic States in Incommensurate Double-Walled Carbon Nanotubes. *Nat. Phys.* **2014**, *10* (10), 737−742.
(33) Stetter, A.; Vancea, J.; Back, C. H. Determination of the Intershell Conductance in a Multiwall Carbon Nanotube. *Appl. Phys. Lett.* **2008**, *93* (17), 172103.
(34) Stetter, A.; Vancea, J.; Back, C. H. Conductivity of Multiwall Carbon Nanotubes: Role of Multiple Shells and Defects. *Phys. Rev. B: Condens. Matter Mater. Phys.* **2010**, *82* (11), 115451.
(35) Levshov, D. I.; Tran, H.-N.; Michel, T.; Cao, T. T.; Nguyen, V. C.; Arenal, R.; Popov, V. N.; Sauvajol, J.-L.; Zahab, A.-A.; Paillet, M. Interlayer Interaction Effects on the G Modes in Double-Walled Carbon Nanotubes With Different Electronic Configurations. *Phys. Status Solidi B* **2017**, *254* (11), 1700251.
(36) Stahl, H.; Appenzeller, J.; Martel, R.; Avouris, P.; Lengeler, B. Intertube Coupling in Ropes of Single-Wall Carbon Nanotubes. *Phys. Rev. Lett.* **2000**, *85* (24), 5186−5189.
(37) Maarouf, A. A.; Kane, C. L.; Mele, E. J. Electronic Structure of Carbon Nanotube Ropes. *Phys. Rev. B: Condens. Matter Mater. Phys.* **2000**, *61* (16), 11156−11165.
(38) Reich, S.; Thomsen, C.; Ordejón, P. Electronic Band Structure of Isolated and Bundled Carbon Nanotubes. *Phys. Rev. B: Condens. Matter Mater. Phys.* **2002**, *65* (15), 155411.
(39) Shi, W.; Wang, Z.; Zhang, Q.; Zheng, Y.; Ieong, C.; He, M.; Lortz, R.; Cai, Y.; Wang, N.; Zhang, T.; et al. Superconductivity in Bundles of Double-Wall Carbon Nanotubes. *Sci. Rep.* **2012**, *2*, 1−7.
(40) Yakobson, B. I.; Couchman, L. S. Persistence Length and Nanomechanics of Random Bundles of Nanotubes. *J. Nanopart. Res.* **2006**, *8* (1), 105−110.
(41) Jiao, L.; Fan, B.; Xian, X.; Wu, Z.; Zhang, J.; Liu, Z. Creation of Nanostructures with Poly(Methyl Methacrylate)-Mediated Nanotransfer Printing. *J. Am. Chem. Soc.* **2008**, *130* (38), 12612−12613.
(42) Thomsen, C.; Reich, S. Raman Scattering in Carbon Nanotubes. In *Light Scattering in Solid IX*; Cardona, M., Merlin, R., Eds.; Springer Berlin Heidelberg: Berlin, Heidelberg, 2007; Vol. *108*, pp 115−234. DOI: 10.1007/978-3-540-34436-0_3.
(43) Maultzsch, J.; Telg, H.; Reich, S.; Thomsen, C. Radial Breathing Mode of Single-Walled Carbon Nanotubes: Optical Transition Energies and Chiral-Index Assignment. *Phys. Rev. B* **2005**, *72* (20), 205438.
(44) Reich, S.; Thomsen, C.; Maultzsch, J. *Carbon Nanotubes*; Thomsen, C., Reich, S., Maultzsch, J., Eds.; Wiley-VCH Verlag GmbH: Weinheim, Germany, 2004. DOI: 10.1002/9783527618040.
(45) Levshov, D. I.; Michel, T.; Arenal, R.; Tran, H. N.; Than, T. X.; Paillet, M.; Yuzyuk, Y. I.; Sauvajol, J.-L. Interlayer Dependence of G-Modes in Semiconducting Double-Walled Carbon Nanotubes. *J. Phys. Chem. C* **2015**, *119* (40), 23196−23202.
(46) Popov, V. N.; Levshov, D. I.; Sauvajol, J.-L.; Paillet, M. Computational Study of the Shift of the G Band of Double-Walled Carbon Nanotubes Due to Interlayer Interactions. *Phys. Rev. B: Condens. Matter Mater. Phys.* **2018**, *97* (16), 165417.
(47) Maultzsch, J.; Reich, S.; Thomsen, C. Chirality-Selective Raman Scattering of the D Mode in Carbon Nanotubes. *Phys. Rev. B: Condens. Matter Mater. Phys.* **2001**, *64* (12), 121407.
(48) Araujo, P. T.; Barbosa Neto, N. M.; Chacham, H.; Carara, S. S.; Soares, J. S.; Souza, A. D.; Cançado, L. G.; de Oliveira, A. B.; Batista, R. J. C.; Joselevich, E.; et al. In Situ Atomic Force Microscopy Tip-Induced Deformations and Raman Spectroscopy Characterization of Single-Wall Carbon Nanotubes. *Nano Lett.* **2012**, *12* (8), 4110−4116.
(49) Müssnich, L. C. P. A. M.; Chacham, H.; Soares, J. S.; Barbosa Neto, N. M.; Shadmi, N.; Joselevich, E.; Cançado, L. G.; Jorio, A.

DOI: 10.1021/acs.nanolett.9b03977
Nano Lett. 2020, 20, 953−962

Strain Discontinuity, Avalanche, and Memory in Carbon Nanotube Serpentine Systems. *Nano Lett.* **2015**, *15* (9), 5899−5904.
(50) Maultzsch, J.; Reich, S.; Thomsen, C. Chirality-Selective Raman Scattering of the D Mode in Carbon Nanotubes. *Phys. Rev. B: Condens. Matter Mater. Phys.* **2001**, *64* (12), 121407.
(51) Buongiorno Nardelli, M.; Yakobson, B. I.; Bernholc, J. Mechanism of Strain Release in Carbon Nanotubes. *Phys. Rev. B: Condens. Matter Mater. Phys.* **1998**, *57* (8), R4277−R4280.
(52) Stuart, S. J.; Tutein, A. B.; Harrison, J. A. A Reactive Potential for Hydrocarbons with Intermolecular Interactions. *J. Chem. Phys.* **2000**, *112* (14), 6472−6486.
(53) Liu, K.; Wang, W.; Xu, Z.; Bai, X.; Wang, E.; Yao, Y.; Zhang, J.; Liu, Z. Chirality-Dependent Transport Properties of Double-Walled Nanotubes Measured in Situ on Their Field-Effect Transistors. *J. Am. Chem. Soc.* **2009**, *131* (1), 62−63.
(54) Collins, P. G.; Arnold, M. S.; Avouris, P. Engineering Carbon Nanotubes and Nanotube Circuits Using Electrical Breakdown. *Science* **2001**, *292* (5517), 706−709.
(55) Karousis, N.; Kobayashi, K.; Shinohara, H.; Tagmatarchis, N. Chemically Induced, Thermally Controlled Peel-Off of the External Walls of Double-Walled Carbon Nanotubes. *Small* **2010**, *6* (24), 2826−2831.
(56) Hong, B. H.; Small, J. P.; Purewal, M. S.; Mullokandov, A.; Sfeir, M. Y.; Wang, F.; Lee, J. Y.; Heinz, T. F.; Brus, L. E.; Kim, P.; et al. Extracting Subnanometer Single Shells from Ultralong Multiwalled Carbon Nanotubes. *Proc. Natl. Acad. Sci. U. S. A.* **2005**, *102* (40), 14155−14158.
(57) Zhang, Y.; Zhou, L.; Zhao, S.; Wang, W.; Wang, E.; Liang, W. Electronic Transport Properties of Inner and Outer Shells in near Ohmic-Contacted Double-Walled Carbon Nanotube Transistors. *J. Appl. Phys.* **2014**, *115* (22), 224503.
(58) Sohn, L. L.; Herberg, J. L.; Harteneck, B. D.; Myers, D. R.; Liddle, J. A. Fabrication of an On-Chip NMR Microfluidics Device. *Tenth International Conference on Miniaturized Systems for Chemistry and Life Sciences*; Tokyo, Japan, Japan, 2006; Vol. *1*, pp 1145−1147.
(59) Moazenzadeh, A.; Spengler, N.; Lausecker, R.; Rezvani, A.; Mayer, M.; Korvink, J. G.; Wallrabe, U. Wire Bonded 3D Coils Render Air Core Microtransformers Competitive. *J. Micromech. Microeng.* **2013**, *23* (11), 114020.
(60) Yao, Z.; Kane, C. L.; Dekker, C. High-Field Electrical Transport in Single-Wall Carbon Nanotubes. *Phys. Rev. Lett.* **2000**, *84* (13), 2941−2944.
(61) Grisi, M.; Conley, G. M.; Sommer, P.; Tinembart, J.; Boero, G. A Single-Chip Integrated Transceiver for High Field NMR Magnetometry. *Rev. Sci. Instrum.* **2019**, *90* (1), 015001.
(62) Hirschmann, T. C.; Araujo, P. T.; Muramatsu, H.; Rodriguez-Nieva, J. F.; Seifert, M.; Nielsch, K.; Kim, Y. A.; Dresselhaus, M. S. Role of Intertube Interactions in Double- and Triple-Walled Carbon Nanotubes. *ACS Nano* **2014**, *8* (2), 1330−1341.
(63) MacKerell, A. D.; Bashford, D.; Bellott, M.; Dunbrack, R. L.; Evanseck, J. D.; Field, M. J.; Fischer, S.; Gao, J.; Guo, H.; Ha, S.; et al. All-Atom Empirical Potential for Molecular Modeling and Dynamics Studies of Proteins. *J. Phys. Chem. B* **1998**, *102* (18), 3586−3616.
(64) Plimpton, S. Fast Parallel Algorithms for Short-Range Molecular Dynamics. *J. Comput. Phys.* **1995**, *117* (1), 1−19.

DOI: 10.1021/acs.nanolett.9b03977
Nano Lett. 2020, 20, 953−962